

Magnetic, transport, and structural properties of Fe/Co/Cu/[Co/Ir/Co] sandwiches and Fe/Co/Cu/[Co/Ir] multilayers prepared by ion-beam sputtering

S. Colis*

IPCMS-GEMME, CNRS-UMR 7504, 23 rue du Loess, F-67037 Strasbourg Cedex, France

A. Dinia

IPCMS-GEMME, CNRS-UMR 7504, ULP-ECPM, 23 rue du Loess, F-67037 Strasbourg Cedex, France

C. Mény, P. Panissod, C. Ulhaq-Bouillet, and G. Schmerber

IPCMS-GEMME, CNRS-UMR 7504, 23 rue du Loess, F-67037 Strasbourg Cedex, France

(Received 3 May 2000)

A study of the structure, transport, and magnetic properties of Co/Ir sandwiches prepared by ion-beam sputtering is presented. Oscillations of giant magnetoresistance (GMR) and coupling strength versus the Ir thickness are observed. In the spin-valve-type sandwich, at low Ir spacer thickness a shift is observed between GMR and coupling oscillations. This is due to the presence of a magnetic $\text{Fe}_{5nm}/\text{Co}_{0.5nm}/\text{Cu}_{3nm}$ buffer, which has an important contribution to the spin dependent scattering, and also to the nature of the indirect exchange coupling. The maximum GMR and coupling strength are about 3% and -0.47 erg/cm^2 , respectively. The most interesting result concerns the nature of the indirect exchange coupling as shown by the NMR analysis. This coupling is homogeneous, and consistent with a biquadratic coupling, instead of the usually observed antiferromagnetic coupling. This is further supported by low-temperature magnetization measurements and TEM investigations, which show that the deposited layers are laterally continuous and free of bridges for 0.5-nm Ir spacer layer.

I. INTRODUCTION

Since the discovery of exchange coupling between adjacent ferromagnetic layers through nonmagnetic spacers¹ and the related giant magnetoresistance (GMR),² the study of these systems has received a great deal of attention, because of their considerable fundamental and technological interest. Usually, antiferromagnetically coupled sandwiches and multilayers give rise to a high saturation field and, sometimes, to a high magnetoresistance. However, large saturation fields are not suitable for read heads and sensors applications. To overcome this drawback, van den Berg *et al.*³ have developed a different generation of angular sensors, showing a good performance, in particular for angle and position detection systems. In these hard-soft sensors, the strongly antiferromagnetically coupled sandwich is used to replace the magnetic hard layer, and is called artificial antiferromagnetic (AAF) sandwich. Therefore the achievement of a perfect antiferromagnetic coupling in a sandwich stack is very important for angular sensors. To study this indirect exchange coupling, a large number of combinations of metals has been used, giving rise to systems with oscillatory antiferromagnetic coupling and different coupling strength values. Among these systems, Co/Ru and Co/Rh were found to present very strong-coupling strength, in particular the Co/Rh system, which showed the strongest AF coupling strength ever observed in sandwiches or multilayers.⁴ From the electronic point of view, the Ir spacer was expected to give large AF coupling values. This has been recently confirmed on Co/Ir multilayers prepared using different growth techniques.⁵⁻⁸ However, there is no report, to our knowl-

edge, on the presence of the AF coupling in Co/Ir sandwiches. Moreover, Yanagihara *et al.*⁸ have recently evidenced the presence of a second order, biquadratic, coupling on a 100-period Co/Ir multilayer prepared by molecular beam epitaxy (MBE) on a MgO substrate. Such biquadratic coupling gives rise to an orthogonal alignment between the magnetization vectors of the adjacent layers. This coupling has been earlier observed⁹⁻¹² and different explanations on its origin have been given, like loss of spins,¹⁰ coupling fluctuations,¹¹ or pinholes in the spacer layer.¹² Furthermore, the evidence of this effect was based, in most of these reports, on magnetization curves simulations.

The aim of this paper is to show the presence of an indirect exchange coupling in ion beam sputtered Co/Ir sandwiches, which exhibits a biquadratic and homogeneous exchange coupling feature. The paper is organized as follows. The description of the preparation method and the advantage of the stack design are presented in Sec. II. In Sec. III, room-temperature GMR and magnetization curves are discussed and indicate a possible existence of a biquadratic coupling. This biquadratic coupling is consistent with the NMR measurements (Sec. IV). NMR also provides some information about the concentration profile at the interfaces. Moreover, an investigation by x-ray diffraction (XRD) and TEM of the structure, grain size, and interdiffusion between Co and Ir at the Co/Ir interface is also presented. Finally, in Sec. V simulations of the low-temperature magnetization curves are reported and analyzed in terms of biquadratic coupling.

II. SAMPLE ARCHITECTURE AND EXPERIMENTAL METHOD

Two types of samples have been prepared. First, a series of $\text{Co}_{3nm}/\text{Ir}_x/\text{Co}_{3nm}$ sandwiches was deposited in order to

analyze the variation of GMR and coupling strength with the thickness of the Ir spacer layer. Second, due to the small thickness of the sandwiches, a $[\text{Co}_{3.5\text{nm}}/\text{Ir}_{0.5\text{nm}}]_{10\times}$ multilayer was prepared to investigate the structure of the layers and the morphology of the Co/Ir interfaces.

All samples were deposited at room temperature on a glass substrate covered by a $\text{Fe}_{5\text{nm}}/\text{Co}_{0.5\text{nm}}/\text{Cu}_{3\text{nm}}$ buffer layer. A $\text{Cu}_{2\text{nm}}/\text{Cr}_{2\text{nm}}$ capping layer was used to cover the samples and protect them against oxidation. Since the magnetic and transport properties of the sandwiches are strongly dependent on the morphology of the magnetic/nonmagnetic interfaces, an important effort was made to optimize the surface quality and the structure of these layers. The growth deposition rates and the thickness of the buffer and capping layers were varied in order to improve, as much as possible, the magnetic and transport properties.¹³ The buffer $\text{Fe}_{5\text{nm}}/\text{Co}_{0.5\text{nm}}/\text{Cu}_{3\text{nm}}$ presents the advantage to reduce the surface roughness of the whole stack. Moreover, its magnetic nature gives a contribution to the GMR signal and, as a consequence, an increase in the total GMR is expected. Thus the GMR signal results from two contributions: the first one coming from the AAF Co/Ir/Co sandwich and the second one, called spin-valve GMR, which results from the interaction between the Fe/Co soft buffer layer and the AAF hard layer. As the buffer layer is decoupled from the sandwich, this hard soft system is ideal for magnetic sensors.³

All samples were prepared by ion-beam sputtering (IBS) technique using a two grid Kaufmann¹⁴ ion source. The base pressure was about 5×10^{-9} mbars. The Ar^+ ions are incident on the sputter target at 400 V with an angle of 45° and the beam current was around 5 mA. The growth of the deposited films was monitored by a vibrating quartz crystal oscillator, which is placed close to the substrates. The growth deposition rates were typically 0.75 nm/min for Co, 0.5 nm/min for Ir, 0.65 nm/min for Fe, and 1.7 nm/min for Cu.

The magnetoresistance of the samples was measured using a low-frequency ac lock-in technique, with a conventional four in line gold-plated contacts (CIP “current in-plane” configuration). At room temperature, the measurements were performed up to 17 kOe applied magnetic field, both parallel and perpendicular to the in-plane current direction, in order to detect any anisotropic magnetoresistance contribution.

The magnetization measurements were carried out using an alternating gradient force magnetometer (AGFM) (Ref. 15) and a superconducting quantum interference device (SQUID) magnetometer, respectively, for room-temperature and low-temperature measurements. In both cases, the magnetic field was applied in the plane of the film and reaching a maximum of, respectively, 13 kOe (AGFM) and 50 kOe (SQUID). The AGFM measurements have been performed with the magnetic field parallel to a reference direction and also at several angles with respect to this direction. Since the magnetization curves are superimposed, we deduced that we have no uniaxial anisotropy.

The x-ray measurements were performed using a Siemens powder diffractometer. $\theta/2\theta$ scans were carried out using a parallel monochromatic Co- K_{α_1} radiation. Small-angle x-ray diffraction was used to check the superlattice period length and the superlattice quality.

Nuclear magnetic resonance (NMR) measurements were

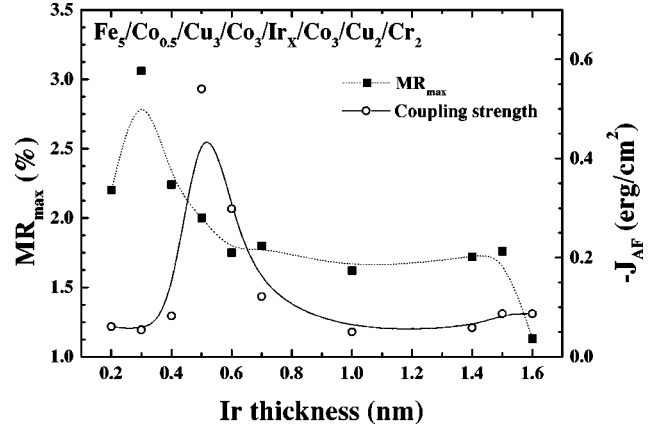


FIG. 1. Magnetoresistance (full squares) and coupling strength (open circles) versus Ir spacer thickness of a $\text{Co}_{3\text{nm}}/\text{Ir}_{X\text{nm}}/\text{Co}_{3\text{nm}}$ sandwich deposited on a $\text{Fe}_{5\text{nm}}/\text{Co}_{0.5\text{nm}}/\text{Cu}_{3\text{nm}}$ buffer layer. The solid and dotted lines are only a guide for the eye.

carried out at 1.5 K on a $\text{Co}_{3\text{nm}}/\text{Ir}_{0.5\text{nm}}/\text{Co}_{3\text{nm}}$ sandwich and a $[\text{Co}_{3.5\text{nm}}/\text{Ir}_{0.5\text{nm}}]_{10\times}$ multilayer, using a broadband automated spectrometer. Measurements have been taken as a function of the applied radio frequency (RF) field H_1 strength, at frequencies between 50 and 250 MHz. A three-dimensional (3D) surface, intensity as a function of both frequency and H_1 strength, is then obtained. The advantage of this method is to visualize the structural inhomogeneities, along the frequency axis, and the magnetic inhomogeneities, along the rf field axis.

Finally, transmission electron microscopy (TEM) observations were carried out using a Topcon EM002B standard microscope, which operates up to 200 kV with a point to point resolution of 0.18 nm. Specimens were prepared using standard technique of mechanical thinning combined with Ar ion-beam etching.

III. MAGNETIC AND TRANSPORT PROPERTIES

A. Sandwiches

To study the magnetic and transport properties, a series of symmetrical sandwiches with a variable Ir thickness has been prepared. The deposited stack presents the following structure: $\text{Fe}_{5\text{nm}}/\text{Co}_{0.5\text{nm}}/\text{Cu}_{3\text{nm}}/\text{Co}_{3\text{nm}}/\text{Ir}_{X\text{nm}}/\text{Co}_{3\text{nm}}/\text{Cu}_{2\text{nm}}/\text{Cr}_{2\text{nm}}$. Oscillations of GMR and exchange coupling strength vs Ir spacer thickness⁵ have been observed and reported in Fig. 1. As clearly seen, the first maximum in the GMR and the exchange coupling do not occur at the same Ir spacer layer thickness. The first maximum of the coupling strength and of the GMR appear at, respectively, 0.5 and 0.3 nm of Ir. From the theoretical point of view, the coupling strength should present a maximum for one monolayer spacer thickness,¹⁷ but experimentally this is hard to achieve, because of the easy mixing of the Co and Ir at the Co/Ir interfaces. Below a certain Ir thickness, bridges appear across the spacer and the direct coupling between the two Co layers favors the ferromagnetic (FM) coupling, instead of the anti-ferromagnetic (AF) coupling, lowering the intensity of the indirect exchange coupling.

We will try now to understand the origin of the shift between the GMR and the coupling strength oscillations. It is

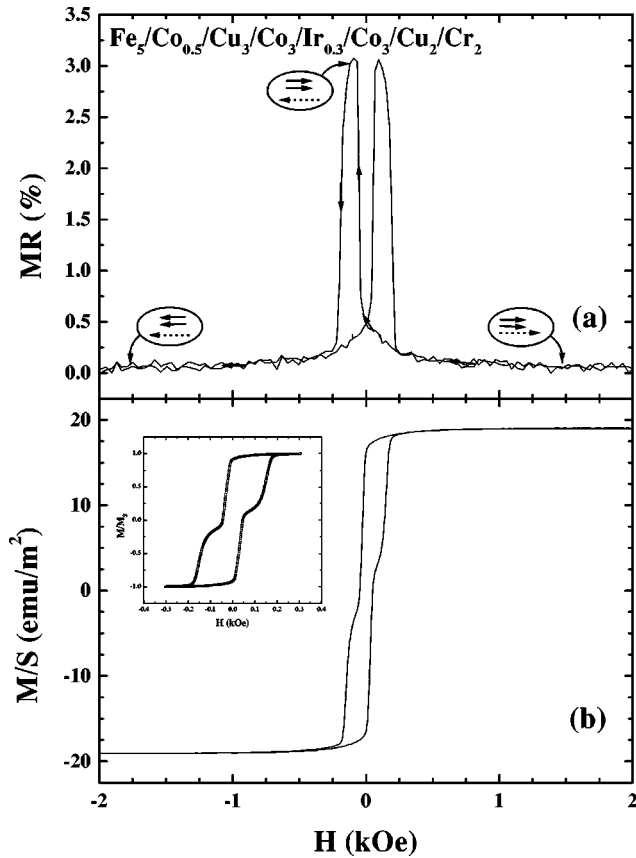


FIG. 2. Room-temperature magnetoresistance [(a) current in-plane configuration] and magnetization (b) curves of a $\text{Co}_{3\text{nm}}/\text{Ir}_{0.3\text{nm}}/\text{Co}_{3\text{nm}}$ sandwich. The magnetic applied field was parallel to the film plane. The dotted arrows correspond to the magnetization of the buffer, while the full arrows correspond to the magnetization of the two Co layers of the trilayer.

important to note first that this effect is observed due to the presence of the soft magnetic Fe/Co layers in the buffer. This adds an interesting contribution to the spin-dependent scattering mechanism. Thus we have to examine carefully the magnetization and the GMR curves for ferromagnetic and antiferromagnetic sandwiches.

For very thin Ir spacer layers, the coupling is ferromagnetic as shown in Fig. 2 for the $\text{Co}_{3\text{nm}}/\text{Ir}_{0.3\text{nm}}/\text{Co}_{3\text{nm}}$ sandwich. Therefore, the contribution to the GMR comes mainly from the spin-dependent scattering due to the different orientations of the soft magnetic buffer layers, with respect to the magnetization of the whole Co/Ir/Co sandwich. This is similar to a hard/soft structure, where the Fe/Co layer in the buffer and the Co/Ir/Co sandwich are, respectively, the soft and the hard layers. As shown in Fig. 2 using arrows, after reversing the magnetic field, the magnetization vector of the soft buffer is switched from the parallel configuration, with respect to the magnetization vectors of the Co layers in the sandwich, to the antiparallel configuration. Such a 180° rotation will give rise to the maximum GMR that can be obtained, which is about 3%.

Increasing the thickness of the Ir spacer layer, the exchange coupling is increased to reach its maximum around 0.5-nm Ir spacer layer. If we suppose in this case that the coupling between the Co layers through Ir is perfect and antiferromagnetic,⁵ the magnetization vectors of the adjacent

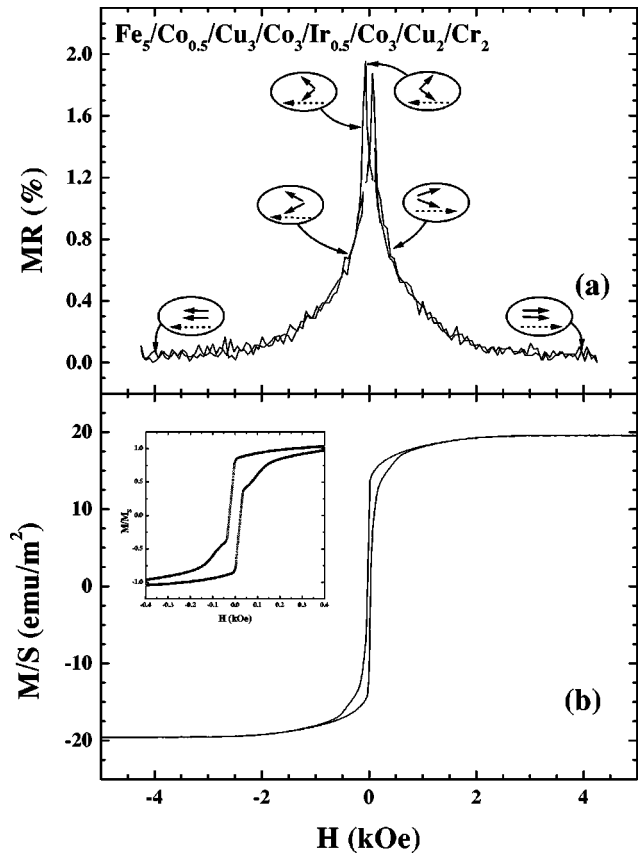


FIG. 3. Room-temperature magnetoresistance [(a) current in-plane configuration] and magnetization (b) curves of a $\text{Co}_{3\text{nm}}/\text{Ir}_{0.5\text{nm}}/\text{Co}_{3\text{nm}}$ sandwich. The magnetic applied field was parallel to the film plane. The dotted arrows correspond to the magnetization of the buffer, while the full arrows correspond to the magnetization of the two Co layers of the trilayer.

Co layers are antiparallel and contained in the film plane, at zero field. After reversing the applied magnetic field, the magnetization vector of the soft buffer layers should rotate by 180° , from the parallel to the antiparallel configuration (or vice versa) with respect to the next Co magnetization vector. In this situation the bottom Co layer of the sandwich will be antiparallel to both the top Co layer and the detection one. In addition, if we consider that the resistance of the sample does not change significantly with the deposition of an additional Ir monolayer (0.5-nm Ir compared to 0.3 nm for the ferromagnetically coupled sandwich), this situation leads to a spin-valve GMR contribution, which is slightly lower than the previous one, in the ferromagnetic sandwich. Thus, adding to this signal, the GMR contribution due to the AAF Co/Ir/Co sandwich, the total GMR signal in the antiferromagnetic sandwich should be close, or slightly higher, to the GMR in the ferromagnetic sandwich. Surprisingly, this is in contradiction with what is experimentally observed. Indeed, the GMR value of the $\text{Fe}_{5\text{nm}}/\text{Co}_{0.5\text{nm}}/\text{Cu}_{3\text{nm}}/\text{Co}_{3\text{nm}}/\text{Ir}_{0.5\text{nm}}/\text{Co}_{3\text{nm}}$ stack, corresponding to the first maximum in the coupling oscillation, reported in Fig. 3 is lower by 40% than the GMR value obtained for the ferromagnetically coupled sandwich.

A reduction up to 15% in the GMR amplitude for the strongly exchange coupled Co/Ir/Co sandwich can, however, be explained if the indirect exchange coupling has a biqua-

dratic nature. This can be calculated using the following expression:^{16,25} $MR \sim \frac{1}{2}(1 - \cos \theta)$, where θ is the angle between the moment of the bottom Co layer of the sandwich and the moment of the Fe/Co layer of the buffer. For the ferromagnetic (0.3 nm of Ir) and the biquadratic (0.5 nm of Ir) coupling, θ is, respectively, 180° and 135° . Moreover, a reduction up to 50% can also be explained considering both the presence of biquadratic coupling and simultaneous rotation of the buffer and sandwich magnetizations. The simultaneous rotation of the buffer and the sandwich net moments is more likely to occur in the case of the sandwich with 0.5-nm Ir than in the sandwich with 0.3-nm Ir. Indeed, simulations of the magnetization have shown that with a given anisotropy, the coercive field is sensitively reduced by the presence of a small biquadratic coupling, compared to the case without coupling. Therefore the coercive fields of the sandwich and the buffer layers are close to each other. Furthermore, the absence of a plateau and of a maximum at zero field in the magnetoresistance curve indicate that there is no well defined antiferromagnetic state. In addition, around zero field, the variation of the resistivity against the magnetic field follows a steep variation, instead of a parabolic one, as expected for a perfect antiferromagnetic coupling. On the basis of the above analysis we can conclude that the presence of biquadratic coupling qualitatively explains the GMR results.

Therefore we have to look carefully to the magnetization curve for the same sandwich, reported in Fig. 3, in order to have a more precise idea on the nature of the exchange coupling. The figure shows a steep increase of the magnetization up to about 0.7 times its saturation value, followed by a slow uptake to the saturation. This high remanence is more important than the one expected from the Fe/Co detection layer and cannot be attributed to errors in the layers thickness evaluation. The existence of a non-negligible difference between the expected and the measured remanence value can, however, be explained by the presence of a biquadratic exchange coupling.

To have an idea on the exchange coupling strength, calculations have been done using the formula: $-J = H_S \cdot (M_R - M_S) \cdot t_{Co}/2$, where H_S is the saturation field, M_R and M_S the remanent and, respectively, the saturation magnetization and t_{Co} the thickness of one Co layer. The maximum coupling strength is obtained for 0.5-nm Ir thickness and corresponds to 0.54 erg/cm^2 . This value is certainly overestimated since it corresponds to a linear variation of the magnetization until the saturation. This is far from our magnetization curve, showing a large remanence and a strong curvature below the saturation. On one hand such a shape of the magnetization loop could result from an inhomogeneity of the magnetic anisotropy within the layers, and/or a large scale lateral inhomogeneity of the coupling strength between the layers. On the other hand such a shape is also expected in the case of biquadratic coupling. However, the GMR observations quoted above and the NMR results that will be presented later favor the last hypothesis. Nevertheless, our values are smaller than the values reported on Co/Ir multilayers⁵⁻⁸ and evidences the difficulty to obtain sandwich stack with a high and perfect indirect exchange coupling. However, the GMR value of this sandwich is about 2%, which is seven times larger than the one measured on Co/Ir multilayers deposited

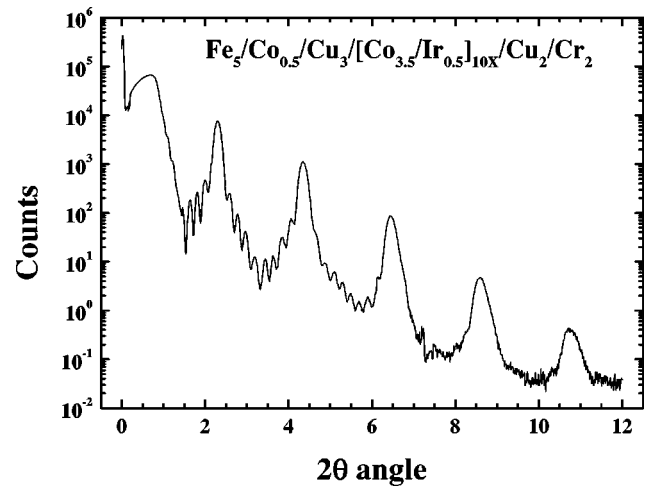


FIG. 4. Low angle x-ray-diffraction pattern spectra for a $[\text{Co}_{3.5\text{nm}}/\text{Ir}_{0.5\text{nm}}]_{10\times}$ multilayer recorded at room temperature using the Cu radiation with $\lambda_{\text{Cu}\alpha_1} = 0.154 \text{ nm}$.

by the same technique (0.3%).⁵ This can, however, be explained by the strong contribution to the GMR coming from the magnetic Fe/Co buffer.

B. Multilayers

In order to study the properties of the Co/Ir stack itself, magnetization and resistivity measurements were performed also on the $[\text{Co}_{3.5\text{nm}}/\text{Ir}_{0.5\text{nm}}]_{10\times}$ multilayer, where the influence of the buffer layer is largely reduced. If the magnetization loop does not differ much from the one of the sandwich with the same Ir thickness, the GMR curve is, however, different due to the strong decrease of the buffer contribution. The GMR ratio for this multilayer is of 0.5%, which is four times less than the sandwich value, but still larger than the value obtained for Co/Ir multilayers deposited by the same IBS (Ref. 5) technique on a Fe/Ir buffer. This demonstrates again the importance of the nature of the buffer layers on the properties of our samples. The shape of the GMR loop of the multilayer is very close to those of sandwiches, but both of them are still far from a parabolic variation. This indicates that the magnetic and transport properties of the sandwiches and multilayers are similar.

The GMR and magnetization curves analysis developed above gives a qualitative indication of the existence of a biquadratic coupling in our sandwiches. However, since the structure and the morphology of the interfaces of thin films and multilayers¹⁸ have a strong influence on the exchange coupling and on the GMR, a detailed structural study of our samples is therefore very important to understand the physical origin of the magnetotransport properties.

IV. STRUCTURE AND INTERFACE INVESTIGATIONS

A. XRD measurements

Due to the small thickness of the layers, x-ray diffraction does not allow us to see any diffraction peak for a sandwich stack. For this reason, x-ray-diffraction measurements have been performed on a $[\text{Co}_{3.5\text{nm}}/\text{Ir}_{0.5\text{nm}}]_{10\times}$ multilayer, in order to obtain information on the quality of the interfaces. All the diffraction patterns were obtained with the scattering vec-

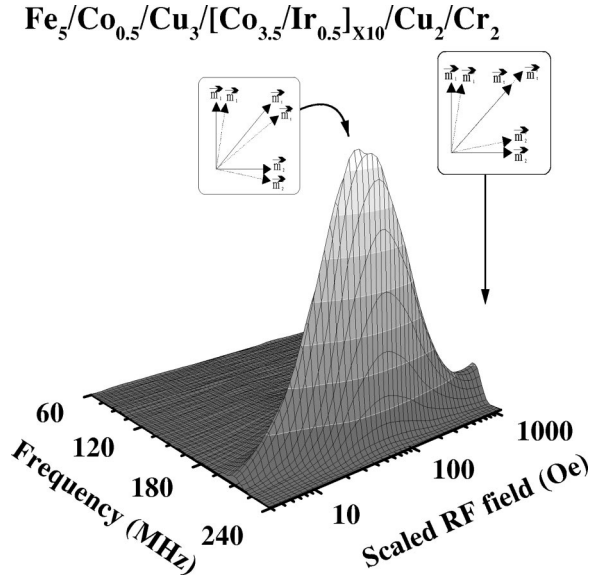


FIG. 5. NMR signal intensity as a function of frequency and rf field as observed in a $[\text{Co}_{3.5\text{nm}}/\text{Ir}_{0.5\text{nm}}]_{10\times}$ multilayer. The narrow distribution of the rf field evidences the presence of an homogeneous coupling. Insets show the oscillations of the magnetization vectors of the two adjacent Co layers, which correspond to the two vibration modes. The “scaled rf field” is the actual rf field value multiplied, for convenience, by an instrumental factor such that the restoring field is read directly as the “scaled rf field” value for the maximum signal. The curves along this axis reflect coarsely the restoring field distribution.²¹

tor perpendicular to the film plane. Figure 4 shows the small-angle x-ray-diffraction spectrum. The presence of the Bragg peaks and the Kiessig fringes is an indication of a small range roughness of the interfaces quality, with a well defined periodicity. From the Bragg peaks, we determine the super-lattice period, which gives rise to an average value of 4.2 ± 0.1 nm. This is in good agreement with the nominal one ($\Lambda = 4$ nm).

B. NMR measurements

In order to understand the origin of the observed inter-layer exchange coupling and its nature, NMR measurements were performed at low temperature on a $[\text{Co}_{3.5\text{nm}}/\text{Ir}_{0.5\text{nm}}]_{10\times}$ multilayer and on a $\text{Co}_{3\text{nm}}/\text{Ir}_{0.5\text{nm}}/\text{Co}_{3\text{nm}}$ sandwich. The spectra were recorded for different values of the excitation radio-frequency (rf) field, a method which allows us to measure the restoring field (anisotropy and/or exchange field) acting on the magnetic moments.^{19,20}

1. Multilayers

The observed NMR intensity vs frequency (f) and rf field (H_1) for the multilayer is presented in Fig. 5 as a 3D surface. In such a picture, the intensity distribution along the frequency axis reflects the structure of the Co layer and its interfaces, whereas the intensity distribution along the rf field axis reflects the distribution of the restoring (coupling and/or anisotropy) field (H_{res}). In the raw NMR data, the restoring field distribution is convoluted with the nuclear-spin response to the rf field, which leads to an intrinsic, “natural” width. Within this resolution, a single peak is observed in the

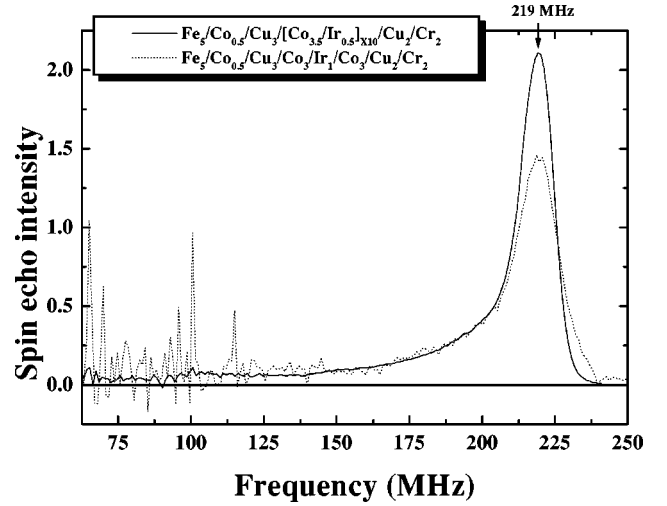


FIG. 6. NMR spectra (normalized to the sample total interface surface area) of a $[\text{Co}_{3.5\text{nm}}/\text{Ir}_{0.5\text{nm}}]_{10\times}$ multilayer (solid line) and of a $\text{Co}_{3\text{nm}}/\text{Ir}_{0.5\text{nm}}/\text{Co}_{3\text{nm}}$ sandwich (dotted line). The width at the half maximum of the main lines and the tails of both spectra are identical, which reflects similar structures and similar Co/Ir interfaces.

present samples, whereas largely inhomogeneous samples would exhibit a much flatter distribution over several orders of magnitude of the field strength (see Fig. 10 of Ref 20).^{19,23} This shows that all the electronic moments magnetize coherently, over the whole stack in low field, as expected for a homogeneous ferromagnet. However, the experimental curves exhibit also an upturn for the largest values of the excitation field, close to the maximum available on the spectrometer. This shows the existence of a second oscillation mode of the electronic moments in large fields. The existence of two oscillation modes, with very different restoring fields, is indeed possible if a bi-quadratic coupling exists between the two adjacent Co layers. In the first vibration mode, for low values of the rf field, the Co moments of the two layers oscillate in phase, keeping constant the 90° angle between them, and the measured restoring field corresponds to the magnetic anisotropy only. In the second mode, the moments of the two layers oscillate in phase opposition, and the measured restoring field arises from both the magnetic anisotropy and the exchange coupling.

Although they are related, these two modes should not be confused with the “symmetric” and “antisymmetric” modes observed by ferromagnetic resonance (FMR) in anti-ferromagnetic materials. Owing to the low excitation frequency the electronic spins are far from resonance and they follow adiabatically the external NMR rf field: from the nucleus viewpoint the electronic spins are essentially nutating. A direct consequence is that the “symmetric” mode is not observed in a purely antiferromagnetic system because the in-phase mutation of the electronic moments cannot be excited by the rf field in the absence of a net magnetization. Only the “antisymmetric” mode, corresponding to the transverse susceptibility of the antiferromagnet, can be observed. The situation is, of course, different in case of noncollinear coupling where the net electronic moment is driven in oscillation by the rf field.

The NMR spectra, corrected for enhancement factor^{19,20,22} of the $[\text{Co}_{3.5\text{nm}}/\text{Ir}_{0.5\text{nm}}]_{10\times}$ multilayer, is reported in Fig. 6.

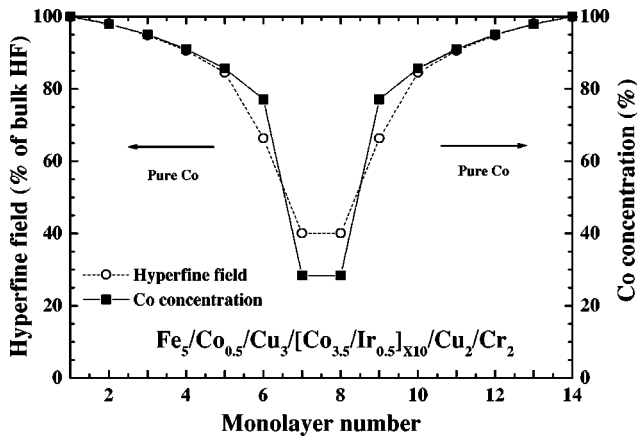


FIG. 7. Concentration and hyperfine field profile of Co atoms across an 0.5-nm Ir spacer layer for the $\text{Co}_{3\text{nm}}/\text{Ir}_{1\text{nm}}/\text{Co}_{3\text{nm}}$ sandwich.

The hyperfine field (H_{HF}), the concentration profile at the interfaces and the structure of the bulk Co layer have been deduced. Generally, an NMR spectrum of a Co/X system, presents a main peak, which corresponds to the bulk Co layers, while the low-frequency tail corresponds to the Co atoms from the grain boundaries and from interfaces, which have different chemical environment. The frequency of bulk Co atoms is expected to be around 226 MHz for a (0001) hcp sample with an in-plane magnetization and at 220 MHz for hcp Co with the magnetization along the c axis. The frequency for fcc Co is expected at 217 MHz.

In our case the NMR spectrum of the multilayer presents a main resonance line at 219 MHz. This cannot be attributed to hcp Co with the magnetization along the c axis since the magnetization measurements have clearly evidenced that the magnetization lies in the film plane. Therefore this resonance frequency is intermediate between the NMR frequency of the fcc and the hcp structures, which means that there is no well defined structure. Moreover, the width at the half maximum of this resonance line is large, which can be explained by the presence of stacking faults. The simulation has allowed us to extract the amount of stacking faults, which is around 48%. This is a clear evidence of the absence of a defined structure. On the other hand, the concentration profile of the Co atoms at the interfaces is presented in Fig. 7. As expected, the Co/Ir interface is strongly interdiffused and it extends over five monolayers. Moreover, the concentration of Co atoms in the middle of the Ir spacer is about 30%, and consequently there is no pure Ir atomic plane in the whole stack.

From the contribution of each mixed atomic layer to the total spectrum, it is possible to compute the average hyperfine field value of each layer, which provides an estimate of the average magnetic moment per Co atom in each mixed layer.^{18,24} The magnetization profile normalized to the bulk magnetization is presented in Fig. 7. Co atoms located in the middle of the Ir spacer lose up to 60% of their magnetic moment, and if we express the profile in terms of magnetic dead layer, 0.14 nm of Co are nonmagnetic at each Co/Ir interface. This value is much smaller than the value reported by Dinia⁵ (0.4 nm/interface), in the case of Co/Ir multilayers deposited on a Fe/Ir buffer. This is a proof of the importance of the nature of buffer layer and of the growth conditions on the interface morphology.

2. Sandwiches

It is already known that the roughness of the interfaces can increase, or decrease, with increasing the number of deposited layers, and consequently differences between sandwiches and multilayers can occur. To verify this hypothesis and to give consistency to our study, another NMR spectra has been recorded for a $\text{Co}_{3\text{nm}}/\text{Ir}_{1\text{nm}}/\text{Co}_{3\text{nm}}$ sandwich (the dotted line in Fig. 6). In this figure the spectra are normalized to the total interface surface area of the sample. With such a normalization the NMR spectra of samples with identical interfaces will be superimposed. From the comparison with the multilayer spectrum, interesting observations can be made (i) first, the main resonance line appears at the same frequency (219 MHz), and presents the same width at the half maximum as the multilayer one, which indicates that the structure is exactly the same with a large amount of stacking faults; (ii) second, the low-frequency tails of the two spectra are absolutely identical, which proves the similar character of interfaces for both samples. The shape of the signal coming from interfaces is the same in both structures, which means that Co/Ir interfaces have the same interdiffusion degree in sandwiches and in multilayers. Thus the roughness does not change with increasing the number of deposited layers as will be also confirmed by the TEM observations. Therefore the structural results found for a multilayer apply as well as for a sandwich. Moreover, at low frequencies, there are no peaks coming from the Co/Cu interfaces even if in the sandwich their impact on the total signal is much more important than in the case of the multilayer. This means that Co/Cu interfaces are interdiffused and gives only a small signal over a large frequency range. The Co/Cu interfaces are strongly intermixed almost as Co/Ir ones, this being a particularity of our deposition technique. Nevertheless, Persat²⁵ obtained using classic sputtering, abrupt Co/Cu interfaces with almost zero magnetic dead layer. This is another evidence on the correlation between the deposition technique and the physical properties of the samples.

NMR results have shown a strong interdiffusion at the Co/Ir interfaces, which extends over more than five monolayers. This interdiffusion is probably at the origin of the biquadratic coupling as supported by NMR analysis, in agreement with Slonczewski's loose spin model.¹⁰ He attributes this effect to the magnetic atoms at the interfaces, which are weakly exchange coupled to the rest of the ferromagnetic parts and give rise to a 90° coupling.

C. TEM measurements

Cross section and plan view TEM measurements were performed on both $[\text{Co}_{3.5\text{nm}}/\text{Ir}_{0.5\text{nm}}]_{10\times}$ multilayer and $\text{Co}_{3\text{nm}}/\text{Ir}_{0.5\text{nm}}/\text{Co}_{3\text{nm}}$ sandwich. In this way the local structure, the grain size, and the quality of the interfaces were directly investigated for both samples.

Figure 8 shows a cross section image of the two samples. The contrast is strong between Co and Ir, mainly due to the large difference between their atomic numbers. In contrast, Co, Cu, Fe, and Cr have closer atomic numbers and cannot be well distinguished and therefore the capping and the buffer appear without contrast. However, the period of the multilayer can be precisely measured, giving the value of about 3.8 ± 0.2 nm. This is in good agreement with the nomi-

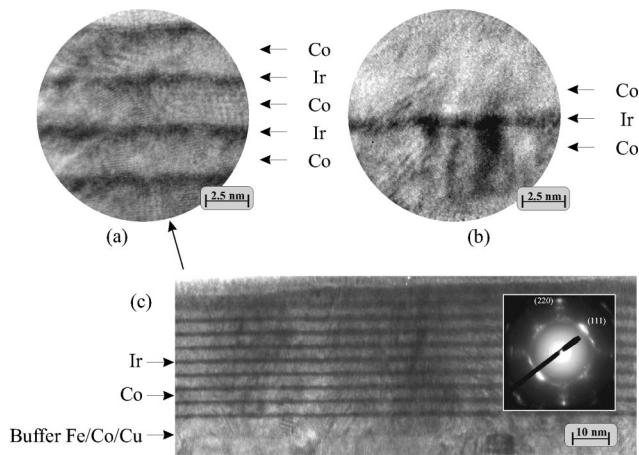


FIG. 8. High-resolution bright-field cross-section TEM images of a $[\text{Co}_{3.5\text{nm}}/\text{Ir}_{0.5\text{nm}}]_{10\times}$ multilayer (a) and (c), and of a $\text{Co}_{3\text{nm}}/\text{Ir}_{0.5\text{nm}}/\text{Co}_{3\text{nm}}$ sandwich (b). The Ir layers (dark bands) appear thicker than 0.5 nm, due to the large interdiffusion at the Co/Ir interfaces. The inset of (c) presents a diffraction image of the cross section. The most intense spots come from the (111) diffraction planes and correspond to a direction which make 45° with the growth direction.

nal value (4 nm). The Ir layers appear to be continuous but their thickness is larger than the nominal value 0.5 nm. This is due to the strong interdiffusion at the Co/Ir interfaces²⁶ as shown by NMR interface profile (Fig. 7). From the contrast analysis between Co and Ir, the Ir layers and the Co/Ir interfaces do not present lateral oscillations and the interfaces roughness do not increase with increasing the number of the

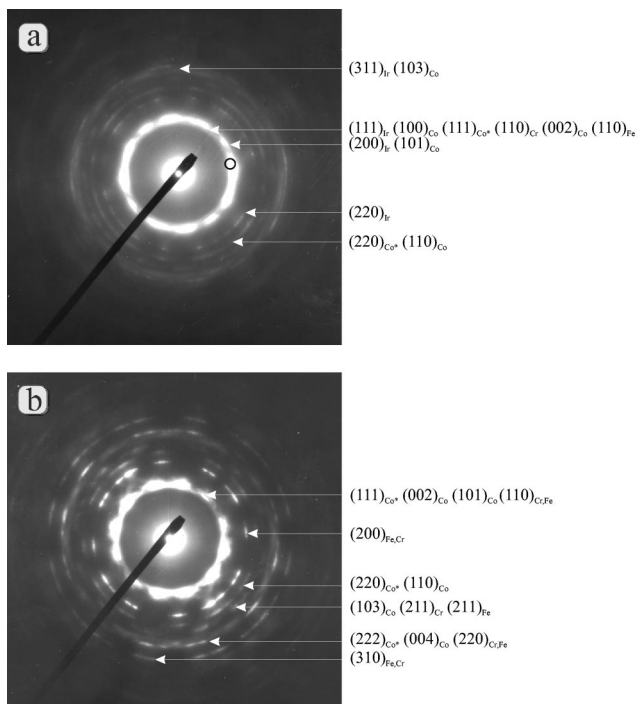


FIG. 9. Diffraction image of a $[\text{Co}_{3.5\text{nm}}/\text{Ir}_{0.5\text{nm}}]_{10\times}$ multilayer (a) and a $\text{Co}_{3\text{nm}}/\text{Ir}_{0.5\text{nm}}/\text{Co}_{3\text{nm}}$ sandwich (b). The small black circle in the region of the most intense diffraction ring (a) indicates the region, where the dark field images were taken. The Co^* indicates the fcc phase of Co.

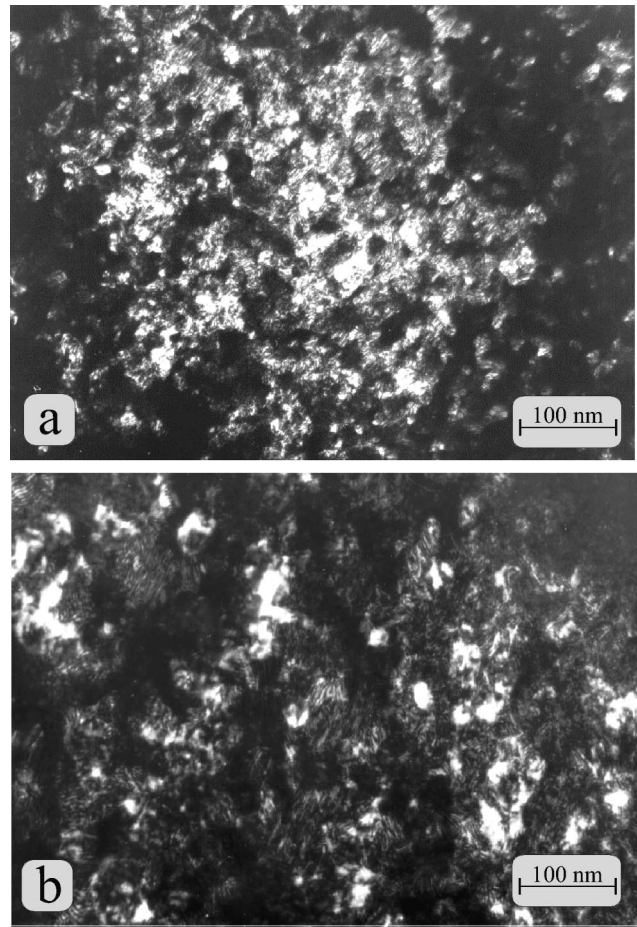


FIG. 10. Dark-field images of a $[\text{Co}_{3.5\text{nm}}/\text{Ir}_{0.5\text{nm}}]_{10\times}$ multilayer (a) and $\text{Co}_{3\text{nm}}/\text{Ir}_{0.5\text{nm}}/\text{Co}_{3\text{nm}}$ sandwich (b). The grains are small, randomly oriented and superposed, which explains the irregular shape of the borders and their diffused contrast.

periods. This is in agreement with the NMR observation that the coupling is homogeneous and free of lateral fluctuations.

A magnification of a high-resolution cross section (XHREM) image of the multilayer shows that there is no coherence between the grains structure along the Z axis. The average coherence length along the Z axis is small and does not exceed 8 nm (maximum two periods). A selected area diffraction pattern (SAD pattern) was also taken in this region and presented in the inset of Fig. 8. The SAD patterns present two types of spots, coming from the superlattice and the atomic planes. The spots along the growth direction are extremely weak and correspond to the (220) diffraction planes. Dark field (DF) images taken under these conditions give a similar size of grains as the values extracted from the XHREM images. The most intense spots come from the (111) planes with the diffraction vector lying at 45° from the growth direction.

The plan view diffraction patterns (Fig. 9) present a series of continuous rings, which are characteristic of polycrystalline samples. This evidences the presence of a well defined crystallographic structure in the grains for both the sandwich and the multilayer. These rings are mainly due to the hcp and fcc Co phases. However, the diffraction rings of the Ir are only observed in the case of the multilayer, mainly due to the larger thickness of Ir, giving rise to a larger diffracted signal.

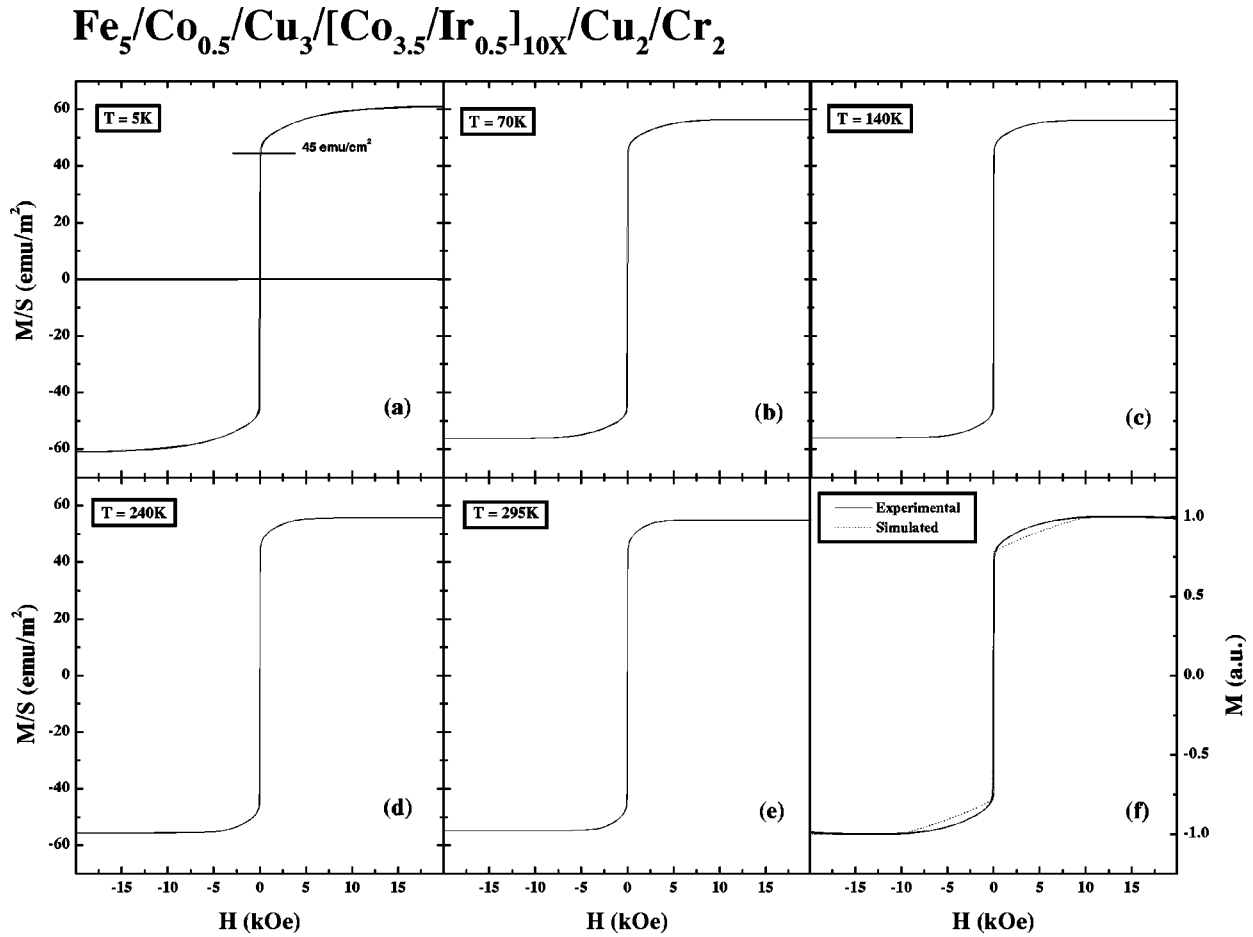


FIG. 11. SQUID magnetization loops on $[\text{Co}_{3.5\text{nm}}/\text{Ir}_{0.5\text{nm}}]_{10\text{X}}$ multilayer recorded at 5, 70, 140, 240, and 295 K [(a)–(e)]. (f) presents the curve from (a) without the buffer contribution (solid line) and the simulation curve with a trilayer model (dotted line).

The dark field images (Fig. 10) were taken in the region of the most intense ring of the plan view diffraction patterns (Fig. 9). This ring is actually the result of the superposition of many rings coming from fcc and hcp Co, Cr, Ir, and Fe, which means that the grains presented in Fig. 10 will correspond to all these materials. The observed grains with regular borders are small, with an average lateral (in-plane) size of about 10 nm, and similar for both samples, in agreement with the cross-section observation. This small size is directly related to our deposition technique.²⁷ On the other hand, most of the white spots of the images are coming from a superposition of grains with almost parallel diffraction planes. This superposition is possible since the small size of the grains along the Z axis is largely below the thickness of the whole stack, and explains very well the irregular shapes of the white spots borders. These spots are more numerous in the case of the multilayer because of the larger number of grains along the Z direction.

Besides the NMR technique, this is another way to show, by direct imaging, that the structural properties and the quality of the interfaces are identical for both the sandwich and the multilayer. As a consequence, the impact of the structure and of the interfaces on the magnetic and transport properties will be the same.

V. LOW-TEMPERATURE MAGNETIZATION MEASUREMENTS AND SIMULATIONS

Temperature-dependent SQUID magnetometry have been performed on the same $[\text{Co}_{3.5\text{nm}}/\text{Ir}_{0.5\text{nm}}]_{10\text{X}}$ multilayer, in order to give another experimental support to the presence of the biquadratic coupling at low temperature as shown by NMR. Measurements were carried out at 5, 70, 140, 240, and 293 K and presented in Figs. 11(a)–11(e).

The first interesting observation is that the saturation field increases strongly with decreasing the temperature. This means that the indirect exchange coupling is largely enhanced at low temperature. This result is also in agreement with Slonczewski's loose spin model,¹⁰ predicting a strong temperature dependence of the 90° coupling, which cannot be easily explained by the fluctuation mechanism. On the other hand, the observed large remanent magnetization excludes the possibility that the indirect exchange coupling is antiferromagnetic. The remanence can be, however, accounted for by considering a pure biquadratic coupling, and by tacking into account the bulk values of the Co and Fe magnetic moments at 5 K (Ref. 28) for magnetization calculation. This leads to values of 45 and 60 emu/m^2 , respectively, for the remanence and the saturation magnetization, which are in very good agreement with the magnetization

curve recorded at 5 K. To have a more precise idea on the strength of the exchange coupling, we tried to simulate the magnetization curve after removing the magnetic buffer contribution, and using a trilayer model [Fig. 11(f)]. The best result was obtained using a ratio $J_{biq}/J_{ferro}=2.3$ ($J_{biq} = -1.55$ erg/cm² and $J_{ferro} = 0.55$ erg/cm²). However, significant differences are evidenced between the roundness of the theoretical and the experimental loop. This can be explained either by the interdiffusion at the Co/Ir interfaces, which leads to a nonperfect biquadratic coupling, or by a magnetic domain structure. Since in the structural analysis, the NMR measurements have clearly evidenced that the coupling is homogeneous, the first hypothesis can be ruled out. However, considering small fluctuations of the coupling and/or fluctuations of the local anisotropy axis, the curvature of the magnetization loop is very well reproduced near the saturation field. In contrast, the differences between the experimental curve and simulation are still important, near zero field. In these conditions, the second explanation seems to be more favorable. Indeed, recently Tiusan²⁹ demonstrated that magnetic walls pinned by structure and/or magnetic defects can be at the origin of this curvature (from zero field up to saturation) of the magnetization loop, and this is very likely to occur in our case since all the samples present a non-negligible amount of structural defects.

VI. CONCLUSION

This study has clearly demonstrated that ion-beam sputtering is suitable to grow Co/Ir/Co sandwiches with biquadratic exchange coupling. TEM observations have shown that the texture is (111), having an angle of 45° with the growth direction, and that the average size of the grains is small particularly along the Z axis. Moreover, NMR and TEM have shown that the Co/Ir interfaces are strongly interdiffused. This interdiffusion, which limits the coupling strength and the GMR ratio, is however at the origin of the main results observed in these sandwiches. Indeed, we have shown that the indirect exchange coupling is biquadratic and homogeneous on the whole film surface. This result is supported by the NMR measurements, the GMR curves, and low-temperature magnetization measurements.

ACKNOWLEDGMENTS

The authors thank R. Poinot for SQUID measurements and T. Romero for technical assistance. This work was partially supported by the European Community “TunelSense” project (Grant No. BRPR-CT98-0657).

*Email address: colis@ipcms.u-strasbg.fr

¹P. Grünberg, R. Schreiber, Y. Pang, M.B. Brodsky, and H. Sowers, *Phys. Rev. Lett.* **57**, 2442 (1986).

²M.N. Baibich, J. Broto, A. Fert, F. Nguyen Van Dau, F. Petroff, P. Etienne, G. Creuzet, A. Friedrich, and J. Chazelas, *Phys. Rev. Lett.* **61**, 2472 (1988).

³H.A.M. van den Berg, W. Clemens, A. Gieres, G. Rupp, M. Vieth, J. Wecker, and S. Zoll, *J. Magn. Magn. Mater.* **165**, 524 (1997).

⁴S. Zoll, A. Dinia, M. Gester, D. Stoeffler, H.A.M. van den Berg, A. Herr, R. Poinot, and H. Rakoto, *J. Magn. Magn. Mater.* **165**, 442 (1997).

⁵A. Dinia, M. Stoeffel, K. Rahmouni, D. Stoeffler, and H.A.M. van den Berg, *Europhys. Lett.* **42**, 331 (1998).

⁶Y. Luo, M. Moske, and K. Samwer, *Europhys. Lett.* **42**, 565 (1998).

⁷H. Yanagihara, K. Petit, M.B. Salamon, E. Kita, and S.S.P. Parkin, *J. Appl. Phys.* **81**, 5197 (1997).

⁸H. Yanagihara, E. Kita, and M.B. Salamon, *Phys. Rev. B* **60**, 12 957 (1999).

⁹C. Chesman, M.A. Lucerna, M.C. de Moura, A. Azevedo, F.M. de Aguiar, S.M. Rezende, and S.S.P. Parkin, *Phys. Rev. B* **58**, 101 (1998).

¹⁰J.C. Slonczewski, *J. Appl. Phys.* **73**, 5957 (1993).

¹¹J.C. Slonczewski, *Phys. Rev. Lett.* **67**, 3172 (1991).

¹²K. Petit, S. Gider, S.S.P. Parkin, and M.B. Salamon, *Phys. Rev. B* **56**, 7819 (1997).

¹³S. Colis, A. Dinia, D. Deck, G. Schmerber, and V. Da Costa, *J. Appl. Phys.* **88**, 1552 (2000).

¹⁴H.R. Kaufmann, J.J. Cuomo, and J.M.E. Harper, *J. Vac. Sci. Technol.* **21**, 725 (1982).

¹⁵P.J. Flanders, *J. Appl. Phys.* **63**, 3940 (1988).

¹⁶B. Dieny, *J. Magn. Magn. Mater.* **136**, 335 (1994).

¹⁷D. Stoeffler and F. Gautier, *J. Magn. Magn. Mater.* **140**, 529 (1995).

¹⁸S. Zoll, A. Dinia, J.P. Jay, C. Mény, G.Z. Pan, A. Michel, L. El Chantal, V. Pierron-Bohnes, and P. Panissod, *Phys. Rev. B* **57**, 4842 (1998).

¹⁹P. Panissod, in *Frontiers in Magnetism of Reduced Dimension Systems*, Vol. 49 of *NATO Advanced Study Institute, Series 3: High Technology*, edited by V.G. Bar'yakhtar, P.E. Wigen, and N.A. Lesnik (Kluwer Academic, Dordrecht, 1998).

²⁰P. Panissod, C. Mény, M. Wójcik, and E. Jedryka, in *Magnetic Ultrathin Films, Multilayers and Surfaces—1997*, edited by J. Tobin, D. Chambliss, D. Rubinski, K. Barmak, P. Dederichs, W. de Jonge, T. Katayama, and A. Schuhl, *MRS Symposia Proceedings No. 475* (Materials Research Society, Pittsburgh, 1997), pp. 157–168.

²¹The scaled RF field is the value $(H_{HF}/H_{1op}) \cdot H_1$, where H_1 is the actual RF field, H_{HF} is the hyperfine field, and H_{1op} is the RF field strength for the maximum signal in a nonmagnetic sample (a calibrated instrumental constant). In a magnetic material the RF field acting on the nuclei is enhanced by the factor H_{HF}/H_{res} , where H_{res} is the restoring field. Consequently the maximum signal is reached for a value H_{1of} of the external RF field such that $(H_{HF}/H_{res}) \cdot H_{1of} = H_{1op}$. The restoring field is then measured by $H_{res} = (H_{HF}/H_{1op}) \cdot H_{1of}$, i.e., the value of the scaled RF field for the maximum signal (see Ref. 20).

²²P. Panissod, J.P. Jay, C. Mény, M. Wójcik, and E. Jedryka, in *Magnetic Ultrathin Films, Multilayers and Surfaces*, edited by A. Fert, H. Fujimori, G. Guntherodt, B. Heinrich, W. F. Egelhoff, Jr., E.E. Marinero, and R.L. White, *MRS Symposia Proceedings No. 384* (Materials Research Society, Pittsburgh, 1995), pp. 61–72.

²³P. Panissod, J.P. Jay, C. Mény, M. Wójcik, and E. Jedryka, *Hyperfine Interact.* **97/98**, 75 (1996).

- ²⁴Y. Henry, C. Mény, A. Dinia, and P. Panissod, *Phys. Rev. B* **47**, 15 037 (1993).
- ²⁵N. Persat, Ph.D. thesis, Louis Pasteur University, Strasbourg, 1998.
- ²⁶T.B. Massalski, *Binary Alloy Phase Diagram*, 2nd ed. (American Society of Metals, Metals Park, OH, 1990), Vol. 2.
- ²⁷A. Dinia, N. Persat, and C. Ulhaq-Bouillet (unpublished).
- ²⁸According to many authors, the values of the magnetic moment at 5 K are around 1440 emu/cm³ for Co and, respectively, 1740 emu/cm³ for Fe. These values were taken from C. Kittel, *Physique de l'état solide*, 5th ed., edited by Bordas (Dunod Université, Paris, 1983), p. 465. Notice that differences of the magnetic moments between the bulk and the thin layer material were evidenced. In our calculations we supposed also that interfaces are abrupt and that there is no loss of magnetic moments at the interfaces.
- ²⁹C. Tiusan, T. Dimopoulos, K. Ounadjela, M. Hehn, H.A.M. van den Berg, V. Da Costa, and Y. Henry, *Phys. Rev. B* **61**, 580 (2000).